Actin filament assembly driven by distributive polymerases clustered on membrane surfaces

R. Dyche Mullins* and Kristen Skruber

Department of Cellular and Molecular Pharmacology
University of California, San Francisco

*Email: dyche.mullins@ucsf.edu

ABSTRACT

Actin filaments created by the Arp2/3 complex form branched networks, that grow and push against cellular membranes. We employ theory and simulation to describe how membrane surfaces accelerate filament assembly via clustering of proteins that bind actin monomers and/or profilin-actin complexes. Briefly, thermal fluctuations drive filament tips on constrained, two-dimensional random walks across the membrane, where they encounter multiple actin-charged polymerases. At low actin concentrations, filament elongation is limited by delivery of monomers to the membrane surface; at high actin concentrations, elongation depends on how quickly fluctuating filaments search the membrane. Surface-mediated polymerization can outpace solution-mediated elongation, even at high actin concentrations (>200 μM). The finite time required for profilin dissociation decreases the advantage conferred by surface-associated polymerases, but only in the absence of force. Load forces enhance the effect of surface polymerases, which can both accelerate elongation and increase the force required to stall filament assembly.

INTRODUCTION:

In eukaryotic cells the actin cytoskeleton moves, shapes, and reinforces cellular membranes. In fact, most actin filaments are created at membrane surfaces (Welch, 2004) where their rapid assembly can generate pushing forces (Mogilner, 1996) that support many cellular processes. Branched actin networks created by the Arp2/3 complex, for example, harness the growth of multiple actin filaments to produce large-scale compressive forces that drive pseudopod protrusion (Bisi, 2013), endocytosis (Mooren, 2012), phagocytosis (Insall, 2009), cell-cell adhesion (Efimova, 2018), cell fusion (Richardson, 2007), healing of membrane ruptures (Clark, 2009), and assembly of autophagosomes (Kast, 2015). Despite the biological importance of actin filament assembly in branched networks, we lack realistic, quantitative models to describe how this process works in living cells or even within complex, reconstituted systems *in vitro*.

A common assumption is that elongation of cellular actin filaments mirrors that of purified actin *in vitro* (Pollard, 2000). Specifically, purified actin forms polarized filaments that elongate when soluble monomers bind to one of their ends. The rates of elongation differ at the two filament ends and also differ depending on whether incoming monomers are bound to ATP or ADP (Pollard, 1986; Fujiwara, 2007). In the cytoplasm most monomeric actin is likely bound to ATP (Rosenblatt, 1995) and complexed with the monomer-binding protein, profilin (Kaiser, 1999). When a profilin-actin complex binds to a free barbed end, the newly attached actin monomer undergoes a rapid conformational change that accelerates profilin dissociation (Pollard, 1984). At relatively low concentrations, therefore, profilin has little effect on the rate of elongation at the fast-growing (*barbed*) end of the filament, but strongly inhibits elongation from the slow-growing (*pointed*) end (Tilney, 1983; Funk, 2019). Based on these observations, the major mode of actin filament elongation in cells is commonly assumed to be the rapid, diffusion-limited (Drenckhahn, 1986) binding of soluble ATP-actin monomers and/or profilin-ATP-actin complexes to free barbed ends (Pollard, 2000).

Many quantitative models of cellular actin assembly explicitly assume that filaments elongate exclusively from soluble building blocks, according to rate constants measured *in vitro*. (Schaus, 2007; Garner, 2022). Unfortunately, few spatially correlated measurements of soluble actin concentrations and filament elongation rates have been made in living cells, and the available data suggest that the relationship between monomer concentration and filament elongation is not so simple (e.g. Koestler, 2009). At least three additional factors affect the rate of filament elongation in cells: (i) physical forces, (ii) the activity of actin polymerases, and (iii) the dissociation of profilin from barbed ends. Physical forces acting on the end of a filament can dramatically slow its growth (Hill, 1982; Mogilner, 1996; Li, 2022); while the activity of actin polymerases can accelerate elongation by several-fold (Romero, 2004; Kovar, 2006; Breitsprecher, 2008; Hansen, 2010; Bieling, 2018). And, ultimately, the rate of profilin dissociation sets an upper limit on the rate of filament elongation (Funk, 2019).

The effect of force is sometimes incorporated into quantitative models of branched actin network assembly (e.g. Schaus, 2007), but the influences of polymerase activity and profilin dissociation are almost universally neglected. This is a problem because the barbed ends of actin filaments in an Arp2/3-generated network generally elongate against membranes coated with a high density of nucleation promoting factors of the WAVE/WASP family. In addition to activating the nucleation activity of the Arp2/3 complex, WAVE/WASP proteins also contain binding sites for monomeric actin and profilin-actin complexes that, when clustered on a surface, work together to create a distributive actin polymerase that can accelerate elongation of nearby filaments by several fold (Bieling, 2018).

Here we provide the mathematical framework for a more realistic description of how actin filaments grow in contact with polymerase-coated membranes. We calculate the rate of membrane-driven filament elongation as a function of both the soluble profilin-actin concentration and polymerase surface density. Using

this result we then compute the relative contributions of soluble and membrane-associated actin monomers to overall filament elongation. Using conservative assumptions, we calculate that more than 50% of actin subunits enter a branched network from surface-associated polymerases, even at high soluble actin concentrations (>200 μM). Filaments begin to interfere with each other and slow the rate of surface-mediated elongation when they come into close enough proximity for their membrane-interaction regions to overlap. Capping proteins, therefore, promote growth of branched actin networks (Hug, 1995; Mejillano, 2004; Iwasa, 2007; Akin, 2008) by decreasing inter-filament competition for surface-bound monomers. Interestingly, profilin dissociation decreases the growth advantage conferred by surface-associated polymerases, especially at high soluble profilin-actin concentrations. When profilin-limited filaments experience a load force, however, polymerase-coated surfaces again confer an advantage, one that increases with increasing force. Finally, under physiologically relevant conditions, we calculate that polymerase-coated membrane surfaces can increase the force required to stall the growth of a nearby actin filament by ~1 pN.

Results

In this section we develop a nanometer-scale model of an actin filament growing near a membrane coated with WAVE/WASP-family proteins. We describe the relevant properties of the membrane surface and the tip of a growing actin filament, and then use these properties to calculate the rate of surface-mediated filament elongation.

Three nucleation promoting factors —WAVE, WASP, and WASH— are conserved across eukaryotic phyla, and likely inherited from the last common ancestor of all eukaryotes (Fritz Laylin, 2017). These proteins and their relatives cluster on membrane surfaces (Figure 1A, 1B) where they direct formation of branched actin networks by locally stimulating Arp2/3-dependent filament nucleation and accelerating filament growth (Machesky, 1999; Bieling, 2018). The actin polymerase activity of WAVE/WASP-family proteins arises from two adjacent sequence motifs, a proline-rich region that binds multiple profilin-actin complexes and at least one WASP homology 2 (WH2) sequence that binds monomeric actin (Figure 1A). We characterize WAVE/WASP proteins on the membrane by specifying three key properties: (i) mode and stoichiometry of actin monomer binding; (ii) mobility on the membrane surface; and (iii) surface density.

WAVE/WASP-family proteins on the membrane. Most monomeric actin in the cytoplasm is likely bound to profilin (Kaiser, 1999), so we will ignore the contribution to polymerase activity of the actin monomer-binding WH2 domains and consider only the profilin-binding, proline-rich regions. Human WAVE1 contains up to six profilin-actin binding sites with a range of measured affinities, from 2 μM to ~200 μM (Bieling, 2018). It is unclear whether six profilins can bind WAVE at the same time but, *in vitro*, profilin:WAVE stoichiometries of at least 2:1 have been detected (Bieling, 2018). This result suggests that the density of polymerizable actin on a WAVE1-coated membrane is at least twice that of WAVE1 itself (Figure 1A).

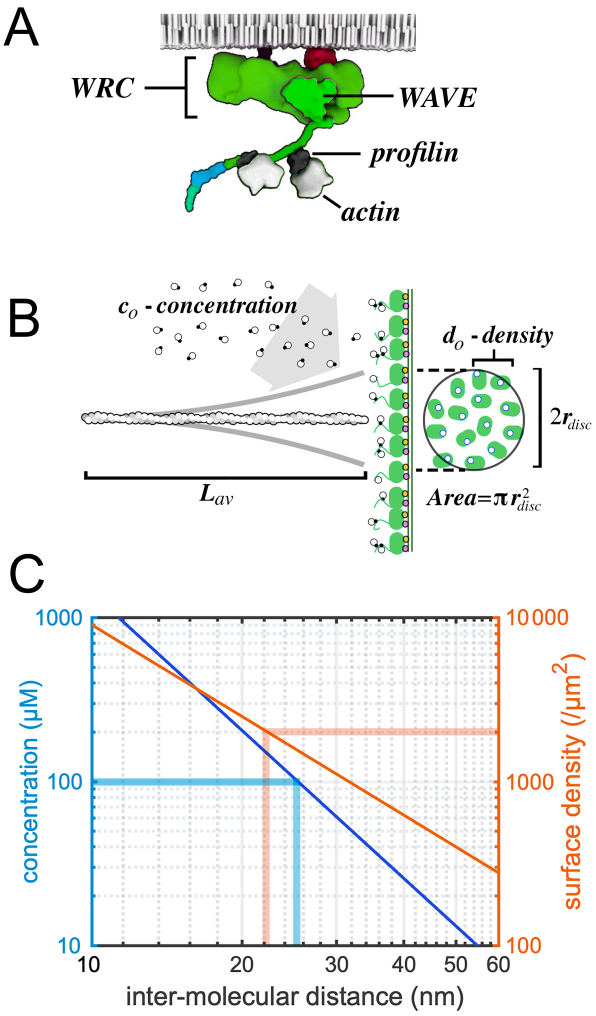

Figure 1. WAVE-family actin polymerases. (A) The WAVE Regulatory Complex (WRC) bound to two profilin actin complexes and attached to a membrane by small G-proteins. (B) Actin filament (length, *Lav*) growing against a WRC-coated membrane with binding sites for profilin-actin (black and white circles; density, d_o,). Thermal fluctuation of the filament (thick gray lines) defines a membrane disc with (radius, r_{disc}) containing multiple polymerases. (C) Log-log plot of solution concentration (blue line and left y-axis) and surface density (orange line and right y-axis) versus average inter-molecular spacing (x-axis). Thick blue lines mark 100 μM and 25 nm. Thick orange lines mark 2000/μm^2 and 22 nm.

WAVE proteins localize to membrane surfaces via interaction with small, rho-family G-proteins (Figure 1A) (Koronakis, 2011). We will ignore lateral motion of these membrane-associated WAVE molecules for two reasons. Firstly, the measured diffusion coefficient of WAVEs on the plasma membrane of a motile cell is an order of magnitude lower than that of nearby actin filament tips (Millius, 2012; Mogilner, 1996). Secondly, our previous *in vitro* experiments demonstrated that lateral mobility of WAVE is not required for polymerase activity (Bieling, 2018).

Estimates of WAVE/WASP protein density on cellular membranes range from >1000/μm^2 for WAVE at the leading edge of crawling neutrophils (Weiner, 2007) to 25,000/μm^2 for WASP at sites of endocytosis in budding yeast (Arasada, 2011). We focus on the lower end of this range and the specific case of mammalian WAVE proteins. WAVEs function as part of a 5-subunit complex, whose overall shape can be approximated as a ~19×8 nm prolate ellipsoid (Figure

1A; Chen, 2010), with a maximum packing density of ~6,600/μm^2 on a membrane surface (Figure 1B). Our analysis, therefore, concentrates on WAVE surface densities of 1,000-6,000/μm^2. As a useful comparison (Huang, 2024), a surface density of 2000/μm^2 reflects an average distance of ~22 nm between WAVE molecules —the same inter-molecular spacing as a three-dimensional solution with a concentration of ~150 μM (Figure 1C).

Filament tip dynamics define a 'footprint' on the membrane. Assuming that WAVE molecules are relatively immobile, the region of membrane that contributes actin monomers to a nearby filament depends mainly on lateral mobility of the filament tip. From theoretical and experimental studies we know that thermal forces cause bending fluctuations in filaments growing against a WAVE-coated surface (Mogilner, 1996; Bieling, 2022). These bending fluctuations cause the tip of the filament to trace a constrained random walk across the surface of the membrane. The shape of the area defined by this random walk depends on the orientation of the filament relative to the membrane and the compressive force acting on it. The tip of an unloaded filament oriented normal to the membrane surface, for example, will trace out a circular disc (Figure 1B). This disc will contain a number of polymerase-bound actin molecules (n_{pol}) that depends on its surface area and the local density of WAVE molecules. Compressive loading will prevent this filament from straightening and decrease the frequency with which its tip visits the center of the disc. Under these conditions the envelope of tip positions will become more annular. In any other orientation the filament tip will trace more elliptical and/or 'croissant' shapes. For simplicity, we begin by considering an unloaded filament oriented normal to the membrane surface. In this case the radius of the membrane interaction disc (r_{disc}) depends only the length and stiffness of the filament.

Estimates of the average filament length in a functional branched actin network range from ~60-300 subunits (~150-800 nm; Svitkina, 1999; Akin, 2008; Koestler,

2009). Here, we assume an average filament length (L_{av}) of ~110 subunits (~300 nm) from free barbed end to network-anchored pointed end. At this length the root-mean square (RMS) displacement of the filament tip due to thermal fluctuations will be ~45 nm (Appendix B). If these filaments grow in proximity to a polymerase-coated membrane (Figure 1B) we define this RMS displacement as the radius of the membrane interaction disc (r_{disc}) —i.e. the 'footprint' of the filament tip on the membrane surface. At densities of 1000-6000/μm^2 the average number of WAVE molecules in this disc will fall between 6 and 36. We limit our analysis to conditions under which the soluble profilin-actin concentration (c_o) significantly exceeds the equilibrium dissociation constant of the two main profilin-actin binding sites on WAVE (2 μM and 4 μM; Bieling, 2018). In which case the average number of polymerizable actin molecules (n_{pol}) within the membrane interaction disc ranges from 12 to 72.

Filament elongation. Surface-mediated filament elongation has different rate-limiting steps in high and low concentrations of soluble profilin-actin. In high concentrations recharging of actin-depleted polymerases from solution is fast, and elongation is limited by the rate at which a thermally fluctuating filament tip encounters surface-bound actin. To calculate this rate we follow Debye and Smoluchowski (Von Smoluchowski, 1917; Debye, 1942) and treat the filament tip as a circular hole whose radius (r_{tip}) represents the effective radius of productive interaction with polymerase-bound actin. We then use Fick's law to calculate the flux of occupied polymerase molecules into the filament-sized hole. This approach is valid regardless of which species —filament or polymerase— undergoes diffusive motion (Debye, 1942). Note also that this calculation represents a two-dimensional 'Smoluchowski limit' on filament elongation, which we denote: R_{2D}. We incorporate steric and electrostatic effects on the elongation rate in a later section.

Across physiologically relevant surface densities of profilin-actin binding sites (d_o), concentrations of soluble profilin-actin (c_o), and tip diffusion coefficients (D_{tip}), the computed interaction rate is well fit by the following formula (Appendix C):

$$R_{2D} \approx \left[2.6 D_{tip} \left(\frac{r_{tip}^2 k_{on} c_o}{D_{tip}} \right)^{0.125} \right] d_o = k' d_o \qquad \textbf{Eqn. 1}$$

Where k'_+ —an effective two-dimensional rate constant— has units of a diffusion coefficient (μm²/sec). This formula reproduces the observed linear dependence of filament elongation on surface density of polymerase sites (Bieling, 2018). Note, however, that even thought the density of polymerase sites (d_o) is fixed, the rate of elongation may be driven arbitrarily high by increasing the soluble profilin-actin concentration (c_o). This behavior reflects the fact that, at very high values of c_o, a polymerase site can collect multiple actin monomers from solution and deliver them to the filament tip during one collision event. The unitless expression in parentheses ($\sim r_{tip}^2 k_{on} c_o / D_{tip}$) is proportional to the number of profilin-actin complexes that can be loaded onto one polymerase during the course of a single collision event. The product $D_{tip} d_o$ is proportional to the filament-polymerase collision frequency at 100% occupancy.

Eqn. 1 provides a two-dimensional analog of the more familiar Smoluchowski limit for filament elongation from soluble monomers (Von Smoluchowski, 1917):

$$R_{soln} = [4\pi D_{pa} r_{tip}]\, c_o = k_+ c_o$$

Note also that **Eqn. 1** assumes free diffusion of the filament tip, but bending mechanics will constrain the tip, mostly to a circular region defined by a radius, r_{disc}. Within this disc, the filament will visit the same polymerase molecules over and over and, when the concentration of soluble profilin-actin is low, this constraint will cause local depletion of polymerase-bound actin. Under these conditions filament elongation will be limited to the rate at which the small number of profilin-actin binding sites (n_{pol}) within the membrane-interaction disc can be refilled. According to Berg and Purcell (1977), this rate is given by:

$$R_{fill} = 4 D_{pa} n_{pol} r_{pa} c_o$$

Where D_{pa} is the diffusion coefficient of soluble profilin-actin and r_{pa} is the capture radius of a polymerase molecule. This equation holds for low polymerase densities. At higher densities, when $n_{pol}r_{pa}>r_{disc}$, the refilling rate will be limited by how quickly profilin-actin can be delivered to the entire membrane interaction disc. Under these conditions the filling rate is independent of the polymerase density and becomes:

$$R_{fill} = 4D_{pa}r_{disc}c_o$$

Assuming a reasonable value of 2 nm for r_{pa}, surface densities above ~3500/μm^2 will cause $n_{pol}r_{pa}>r_{disc}$, so we will use the second expression above for R_{fill} in most of our analysis. Regardless of which expression we use, however, the overall, surface-associated polymerization rate (R_{surf}) satisfies the expression:

$$\frac{1}{R_{surf}} = \frac{1}{R_{fill}} + \frac{1}{R_{2D}}$$

Which yields:

$$R_{surf} = 4\pi D_{pa}r_{tip}c_o\left(\frac{d_o}{ac_o^{7/8} + bd_o}\right) \qquad \textbf{Eqn. 2}$$

With constants, a and b, defined by :

$$a = \frac{4\pi D_{pa}r_{tip}^{0.75}}{2.6D_{tip}^{0.875}k_{on}^{0.125}} \qquad b = \pi\frac{r_{tip}}{n_{pol}r_{pa}}$$

We can now express the rate of surface-mediated interaction (R_{surf}) in terms of the more familiar solution-mediated rate (R_{soln}):

$$R_{surf} = R_{soln}\left(\frac{d_o}{ac_o^{0.875} + bd_o}\right) \qquad \textbf{Eqn. 3}$$

At low profilin-actin concentrations (c_o) the ratio of surface- to solution-mediated elongation rates depends only on the number of actin binding sites that feed each filament and the interaction radii of the polymerase and filament tip:

$$\frac{R_{surf}}{R_{soln}} \approx \frac{1}{b} = \frac{n_{pol}}{\pi}\left(\frac{r_{pa}}{r_{tip}}\right) \qquad \textbf{Eqn. 4a}$$

When profilin-actin concentration is low *and* the surface density of polymerase sites is high (d_o >3500/μm²) the relative elongation rate reduces to the ratio of the radii of the membrane interaction disc and the filament tip:

$$\frac{R_{surf}}{R_{soln}} \approx \frac{1}{b} = \frac{1}{\pi}\left(\frac{r_{disc}}{r_{tip}}\right) \qquad \textbf{Eqn. 4b}$$

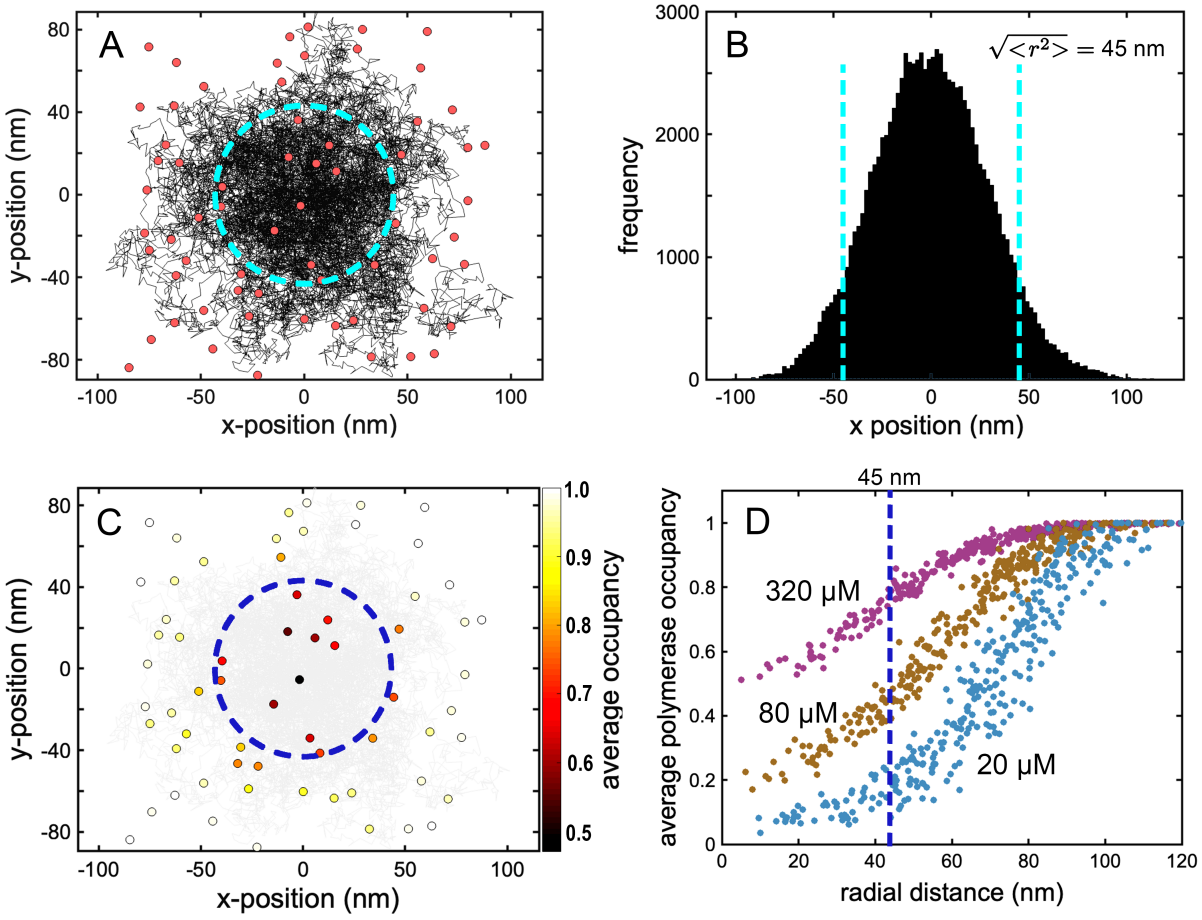

Figure 2. Random walk simulations of filament elongation near a polymerase-coated membrane. (A) Trajectory of a 0.02 second constrained random walk (black) across a 2D surface randomly seeded with polymerase molecules (red circles) at an equivalent of 2000/μm². Dashed cyan circle: RMS radial position of the tip over the trajectory. (B) Histogram of x-projected tip positions. Dashed cyan line: RMS tip position. (C) Polymerase molecules from (A) colored according to average occupancy over a 0.1 sec trajectory. Soluble proflin-actin concentration: 320 μM. (D) Average occupancy over 0.4 second random walks at three different soluble profilin-actin concentrations: 20 μM, 80 μM, and 320 μM, as marked. Each curve is the aggregate of 5 simulations.

The factor of π in **Eqn. 4b** reflects the change from a 3-dimensional target at the end of a filament to a 2-dimensional target on the membrane (Berg, 1977). Given the calculated size of the membrane interaction disc (r_{disc} = 45 nm) and the estimated capture radius for a free barbed end (~2 nm; Drenckhahn, 1986) surface-mediated filament elongation will outpace solution-mediated growth by a maximum of ~7-fold at low actin concentrations and high polymerase densities (>3500/μm^2).

Random walk simulations of surface-mediated polymerization. To test the assumptions underlying our mathematical analysis we constructed a numerical simulation of the tip of an actin filament undergoing a constrained random walk across a polymerase-covered membrane surface (Figure 2A). Briefly, we assumed that the filament tip undergoes a two-dimensional random walk with an effective diffusion coefficient of 4 μm^2/sec (Mogilner, 1996), while experiencing a distance-dependent restoring force directed toward the origin. We chose a spring constant that produces a root-mean-square tip displacement of 45 nm, consistent with thermal fluctuations of a 300 nm actin filament (Figure 1B, B1). We randomly distributed immobile polymerase sites at various densities across the surface, and scored an interaction every time the filament tip ventured within 2 nm (r_{tip}) of an actin-charged polymerase site. To match our diffusion-limit calculations, we counted every interaction as a filament elongation event. Empty polymerase sites that had given up their actin monomer to the filament were replenished at a rate proportional to the concentration of soluble profilin-actin (Berg, 1977).

In our simulations the origin-directed restoring force effectively constrains trajectories to a radially symmetrical region centered on the origin (Figure 2A), and the distribution of tip positions projected onto both x-and y-axes is approximately Gaussian (Figure 2B). As predicted, the constrained nature of the random walk produces a local depletion of actin-charged polymerase molecules, primarily within the membrane interaction radius (Figure 2C), and the extent of this local actin depletion depends on the concentration of soluble profilin-actin

(Figure 2D). In addition to these qualitative features, the quantitative results of random walk simulations fit remarkably well with theory predictions (Figure 3). According to both theory and simulation, surface-mediated elongation "wins" at lower profilin-actin concentrations, while solution-mediated elongation wins at higher concentrations. The crossover point, where surface- and solution-mediated elongation rates are equal, increases with increasing polymerase surface density. At physiologically relevant surface densities these crossover points can significantly exceed ~100 μM (Figure 3B), the soluble actin concentration estimated in many cell types (see Discussion). Quantitative agreement (Figure 3B) is especially remarkable given the lack of free parameters in both the theory and simulation.

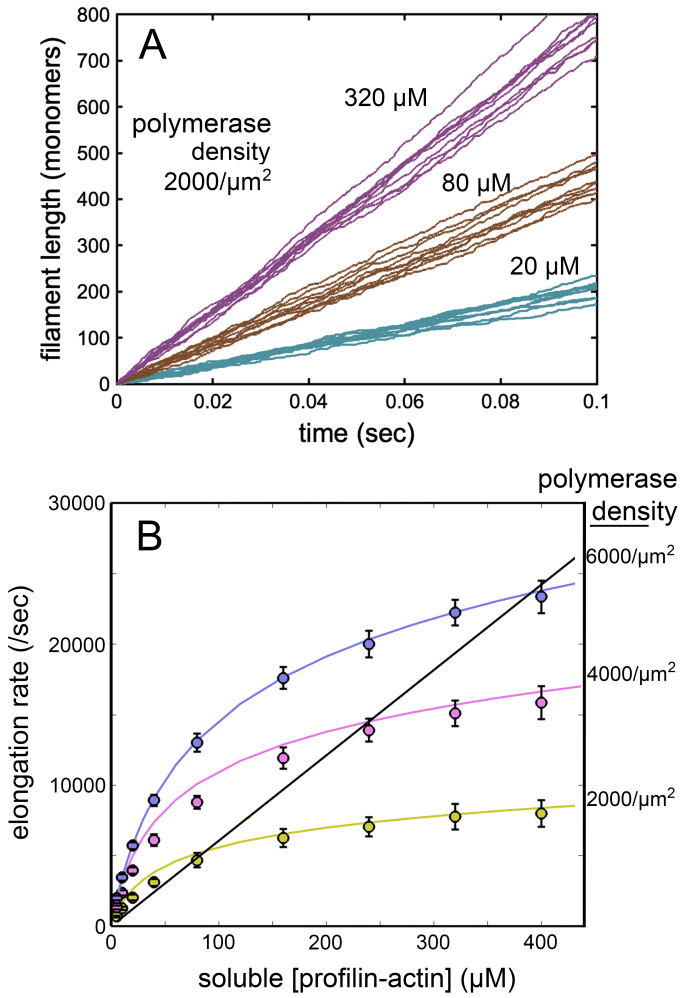

Figure 3. Surface-mediated elongation in random walk simulations. (A) Elongation traces from random walk simulations at three soluble profilin-actin concentrations: 20 μM, 80 μM, and 320 μM (as marked). Lines represent 10 simulations at each concentration. Polymerase surface density: 2000/μm2. (B) Comparison of elongation rates determined from simulation (color-filled circles; error bars: +/- standard deviation of 10 simulations of 0.1 seconds) and theory. Color denotes polymerases density. Yellow: 2000/μm^2; magenta: 4000/μm^2; blue: 6000/μm^2. Solid curves: **Eqn. 2**. Black line: solution-mediated elongation (R_{soln}).

Relative contributions of the solution and the surface. A filament growing against a membrane covered with distributive polymerases will

incorporate *both* soluble and surface-bound monomers. Thus, the total elongation rate will be:

$$R_{total} = R_{surf} + R_{soln} = R_{soln}\left(1 + \frac{d_o}{ac_o^{0.875} + bd_o}\right)$$

Which can be re-arranged into:

$$R_{total} = R_{soln}\left(\frac{ac_o^{0.875} + (b+1)d_o}{ac_o^{0.875} + bd_o}\right) \qquad \textbf{Eqn. 5}$$

Eqn. 5 expresses total elongation rate as a function of the solution-mediated rate. The bracketed term in **Eqn. 5**, therefore, represents fold enhancement of elongation due to the effect of polymerases. The fraction of *total* actin entering the network from the surface is the ratio of polymerase-mediated to total elongation:

$$f_{surf} = \frac{R_{surf}}{R_{total}} = R_{soln}\left(\frac{d_o}{ac_o^{0.875} + (b+1)d_o}\right) \qquad \textbf{Eqn. 6}$$

At an actin binding site density of 4000/μm^2, the soluble profilin-actin concentration at which half the elongation occurs from surface-bound actin (f_{surf} = 0.5) turns out to be ~240 μM. Below this value, more actin enters the network from the surface than from solution. As the soluble profilin-actin concentration approaches 0 μM the ratio of surface- to solution-mediated assembly rates approaches the limiting value given by **Eqn. 4b**, and the fraction of actin delivered from the surface approaches its maximum value of 0.88.

Effects of filament crowding. Previous experimental work revealed an inverse relationship between the local density of growing barbed ends and the elongation rate of actin filaments in a branched network (Akin, 2008; Bieling, 2018; Li, 2022). In our formalism, each filament tip is surrounded by a *radius of interference* (r_{inf}) such that, when the distance between two tips (x_{ff}) is greater than twice this radius (i.e. $x_{ff} > 2r_{inf}$) they will not interact with the same population of polymerases and, therefore, not affect each other's elongation rates. Note that, because fluctuating tip positions are not uniformly distributed across the membrane interaction disc

(defined by r_{disc}) the value of r_{inf} will generally be larger than that of r_{disc} (Figure 4A). When two tips come close to each other ($x_{ff} < 2r_{inf}$) the degree of interference will depend on the degree of overlap. For filaments normal to the membrane, a lens-shaped overlap region with area A_{OL}, contributes a fractional overlap (f_{OL}) of $A_{OL}/\pi r_{inf}^2$.

Given a filament surrounded by n near neighbors, each with a different fractional overlap (i.e. $f_{OL1}, f_{OL2}, f_{OL3}, \ldots, f_{OLn}$), the effective number of competitors, n_{eff}, is given by:

$$n_{eff} = \sum_{i=1}^{n} f_{OLi}$$

The effect of competing filaments will be to reduce the steady-state occupancy of polymerases within the membrane interaction area, and a simple modification to **Eqn. 3** can account for this reduction:

$$R_{surf} = R_{soln}\left(\frac{d_o}{ac_o^{0.875} + [1 + \alpha n_{eff}]bd_o}\right) \qquad \textbf{Eqn. 7}$$

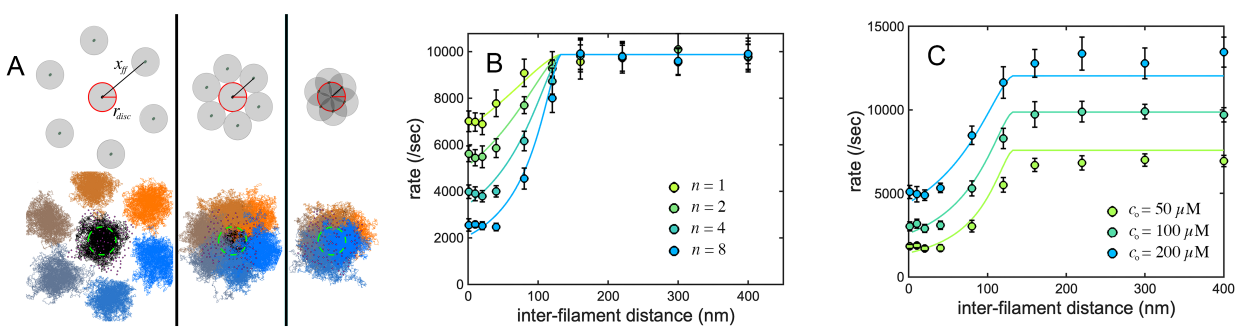

Figure 4. Effect of filament crowding on surface-mediated elongation. (A) Membrane interaction discs (top) and random walk trajectories (bottom) of seven filaments at three inter-filament spacings. (B) Effect of various numbers (n) of competing filaments in c_O=100 μM profilin-actin. (C) Effect of n=6 competitors in various profilin-actin concentrations. (B and C) d_O = 4000/μm^2; competitors radially symmetrical.

Where α is a fitting factor that compensates for non-uniform distribution of tip positions across r_{disc}. This equation agrees well with random walk simulations (Figure 4) when the radius of interference (r_{inf}) is 1.5 times r_{disc} and α has a value of

2. This approach can be generalized to describe different densities and distributions of membrane-proximal filament tips.

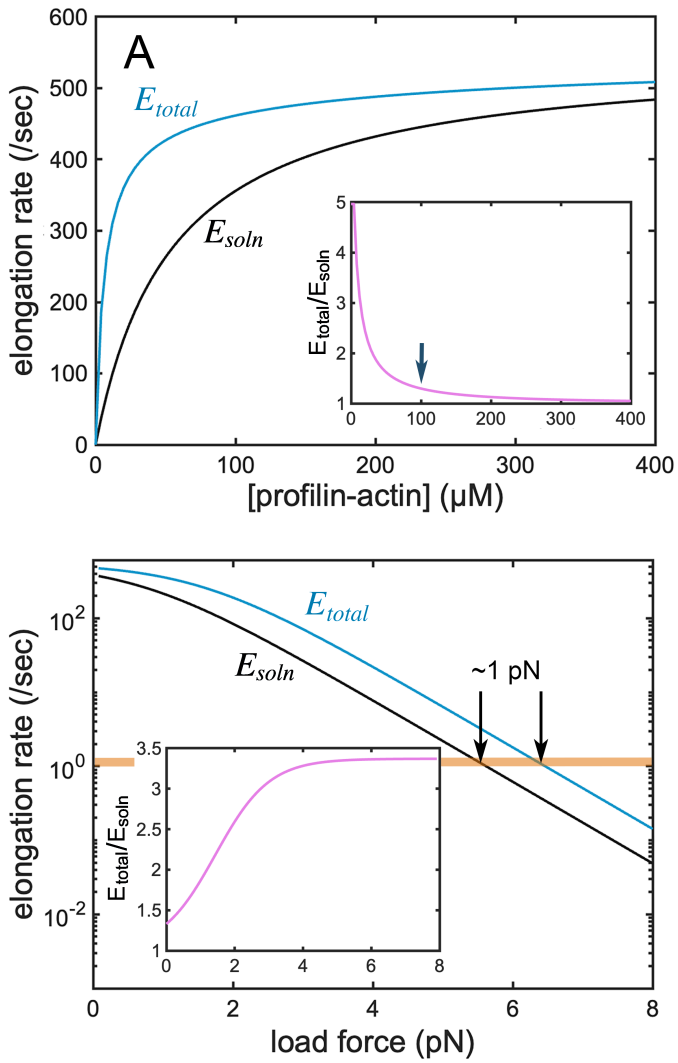

Figure 5. The effects of profilin dissociation and applied force on surface-mediated filament elongation. (A) Filament elongation limited by the rate of profilin dissociation. Black: solution-mediated elongation; blue: solution- plus surface-mediated elongation (d_o=4000/μm^2). Inset: rate enhancement due to polymerase activity. X-axis same as main plot. Arrow marks co=100 μM. (B) Filament growth against a load force. Black: solution-mediated elongation; blue: total (solution- plus surface) elongation (c_o=100 μM; d_o=4000/μm^2). Arrows mark intersection of elongation rate with monomer dissociation rate. Inset: rate enhancement due to polymerase activity. X-axis same as main plot.

Profilin dissociation from barbed ends. Converting the actin component of a profilin-actin complex into a subunit of a growing filament requires several steps (Pollard, 1984). In the first step, a profilin-actin complex binds the filament barbed end. For a short time, the newly attached actin molecule retains its 'monomer' conformation (Kabsch, 1990; Schutt, 1993) and high-affinity interaction with profilin (Bieling, 2018). In less than 0.002 seconds (Funk, 2019), however, the actin shifts to a 'filament' conformation (Oda, 2009), and releases the bound profilin. Because profilin blocks access to the filament barbed end, its dissociation is required for continued elongation and so the rate at which this process occurs sets an ultimate limit on the rate of filament elongation.

Note that our calculations for the

effect of polymerase activity are all based on diffusion-limited encounter rates, so the fraction of monomers that enter from the solution versus the surface are not changed by the effect of profilin. That is, when profilin dissociates from a barbed end, the rates at which it will encounter a new profilin-actin complex from solution versus the surface are unchanged. **Eqn. 6**, therefore, remains valid regardless of the rate of profilin dissociation.

To account for the effect of profilin dissociation we must first convert our diffusion-limited 'monomer-encounter' rates (i.e. R_{surf}, R_{soln}, and R_{total}) to elongation rates, by accounting for steric and electrostatic effects. We estimate an effective steric-and-electrostatic factor (Debye, 1942) for solution-mediated elongation, ϕ_{se}, by dividing measured actin filament elongation rate constants (Pollard, 1986; Fujiwara, 2007) by the Smoluchowski limit calculated above (i.e. R_{soln}). Assuming that steric and electrostatic effects are the same for solution- and surface-mediated polymerization (see Discussion), we apply this same correction factor to all of our calculated rates. The profilin dissociation-limited elongation rates ($E_{soln\text{-}p}$, $E_{surf\text{-}p}$, and $E_{total\text{-}p}$) are now given by:

$$E_{soln-p} = \frac{k_{p-}}{1 + \left(\frac{k_{p-}}{\phi R_{soln}}\right)} \qquad \textbf{Eqn. 8a}$$

$$E_{surf-p} = \frac{k_{p-}}{1 + \left(\frac{k_{p-}}{\phi R_{surf}}\right)} \qquad \textbf{Eqn. 8b}$$

$$E_{total-p} = \frac{k_{p-}}{1 + \left(\frac{k_{p-}}{\phi R_{total}}\right)} \qquad \textbf{Eqn. 8c}$$

Where $k_{p\text{-}}$ —the rate constant governing profilin dissociation— has a measured value of ~550/s, equivalent to the rate of solution-mediated filament elongation in the presence of 55 μM soluble actin. This means that, at cellular profilin-actin concentrations of ~100 μM, filament elongation will occur at a more or less fixed rate, regardless of the influence of surface-associated polymerases (Figure 5A). Note that, even though the polymerase-coated surface may not increase the

elongation rate, more subunits may still be delivered to the filament from the surface than from solution (**Eqn. 6**).

If surface-associated polymerases cannot accelerate filament elongation beyond the speed limit imposed by profilin dissociation, do they have any effect on the rate of network growth? In soluble actin concentrations of ~100 μM and zero load force, the answer appears to be: "not much." When forces are applied to the network, however, the answer is very different.

The effect of force. When an actin filament grows against an opposing force the elongation rate slows by an amount that reflects the energy required to insert each new subunit against the applied force. Specifically, if subunit addition extends the filament length by δ, against opposing force f_o, elongation slows exponentially, according to:

$$e^{\frac{-\delta f_o}{k_B T}}$$

Where k_B is Boltzmann's constant and T is absolute temperature. This factor follows directly from thermodynamic analysis (Hill, 1982), while Elastic Brownian Ratchet theory provides a clear microscopic rationale. Briefly, this factor represents the fraction of exponentially distributed filament fluctuations that are large enough to permit insertion of a δ-sized building block between the filament tip and the load surface (Mogilner, 1996). At room temperature, $k_B T$ is approximately 4.11 pN-nm, and adding a profilin-actin complex to the barbed end of a filament increases its length by ~5.2 nm (i.e. the 2.7 nm actin subunit overlap plus the 2.5 nm length of a bound profilin). The ratio, $\delta/k_B T$, therefore, becomes ~1.27/pN. If we assume that force has little or no effect on the rate of conformational change in the terminal monomer or the dissociation of profilin (Mogilner, 1996), the rates of elongation become:

$$E_{-pf} = \frac{k_{p-}}{1 + \left(\frac{k_{p-}}{\phi R e^{-1.27 f_o}}\right)} \qquad \textbf{Eqn. 9}$$

Assuming realistic values for c_o (100 μM) and d_o (4000/μm^2) we can plot the adjusted rates of surface- and solution-mediated elongation as well as the total elongation rate ($E_{surf\text{-}pf}$, $E_{soln\text{-}pf}$, and $E_{total\text{-}pf}$), as functions of applied force (Figure 5B). Under these conditions the surface-polymerases have a modest (1.3-fold) effect on zero-load elongation. As force increases and elongation rates decrease, however, the effect of the polymerases becomes more pronounced. For forces in the region of 4-7 pN (the estimated range of stall forces for single actin filaments at the leading edge of crawling cells) the polymerase-coated surface enhances elongation by ~3.5-fold (Figure 5B).

Note that when elongation slows to the point where it equals the rate of monomer dissociation (~1/sec) filament growth will stall. For the conditions shown in Figure 5B, surface polymerases increase this force by ~1 pN (~18%).

Discussion

Similar to Edwin Abbott's, "Flatland" (Abbot, 1884), actin filament assembly is a "romance of many dimensions." Soluble profilin-actin complexes, diffusing in three-dimensions, are collected onto a two-dimensional membrane surface by polymerase molecules that facilitate their conversion into one-dimensional filaments. The proline-rich profilin-actin binding sites found on WAVE/WASP family proteins function as the major inter-dimensional portal for assembly of branched actin networks.

Experimentally, the actin polymerase activity of surface-bound WAVE/WASP proteins exhibits two key features: (i) it is highly distributive and (ii) it increases linearly with surface density (Bieling, 2018). The distributive nature of the activity means that a given WAVE/WASP molecule spends very little time bound to the end of a growing filament, while the density dependence indicates that the elongation rate depends on how quickly a filament tip encounters fresh, actin-charged polymerases. In these chance encounters, who finds whom? Do mobile polymerase molecules find a more or less static filament, or does a dynamic filament tip search for nearby polymerases? Our analysis assumes that tip mobility drives the interaction, but our mathematical formalism can also account for polymerase mobility. Similar to the Debye-Smoluchowski equation, we could replace the D_{tip} term in **Eqn. 1** with (D_{tip} + D_{pol}), where D_{pol} represents the diffusion coefficient of the polymerase molecules. We note that polymerase molecules may not undergo long-range motion, but flexible, C-terminal sequences may still permit significant segmental motion of bound profilin-actin complexes. We could account for this by adding an effective interaction radius, r_{pa}, for the polymerase-bound actin to **Eqn. 1**, replacing r_{tip} by (r_{tip} + r_{pa}).

Two-dimensional diffusion of a protein in a lipid membrane is generally much slower than three-dimensional diffusion of a soluble protein (McCloskey, 1986), which is one reason we ignore the lateral diffusion of WAVE molecules in our model. Interestingly, the effective diffusion coefficient calculated by Mogilner and

Oster (1996) for a thermally fluctuating filament tip (4 μm^2/sec) is remarkably similar to the measured diffusion coefficient of profilin-actin in cytoplasm (5 μm^2/sec). Also, at the estimated membrane densities of WAVE/WASP family proteins, the intermolecular spacing of surface-associated actin binding sites (<22 nm) is closer than of actin molecules in a 100 μM solution. These facts, together with the higher probabilities of molecular interaction in two dimensions (Huang, 2024) help explain the ability of clustered WAVE/WASP molecules to accelerate filament assembly, even when the soluble actin concentration is >100 μM.

We assume that steric and electrostatic effects are the same for solution- and surface-mediated elongation. We take this approach partly to demonstrate that invoking these effects is not required to explain the enhancement of polymerization caused by clustering WAVE/WASP proteins on a membrane surface. Formally, the steric factor could either: (i) decrease due to a decreased rotational diffusion coefficient of the tethered profilin-actin (Northrup, 1992); (ii) increase due to reduced dimensionality and increased search efficiency of the tethered species (Windisch, 2006); or (iii) remain unchanged. When future biophysical experiments and/or molecular dynamics simulations provide additional data relevant to this question, we can modify the value of the steric/electrostatic factor in **Eqns 8a**, **8b**, **8c,** and **9**.

In mammalian cells the estimated concentrations of monomeric actin near sites of branched network assembly vary considerably. Many estimates fall in the range of ~100 μM (Mogilner, 2002; Kiuchi, 2011) to 150μM (Koestler, 2009), while some fall as low as 10μM (Novak, 2008) and some as high as 250 μM (Fox, 1993). Our theory and simulations demonstrate that surface-associated polymerases effectively accelerate filament elongation across this entire range of soluble actin concentrations. At low concentrations the rate of surface-mediated polymerization is limited by how quickly the small number of polymerases that interact with each filament (n_{pol}) can be replenished from solution. For a diffusion-limited interaction, this rate depends linearly on the concentration (c_o) and

diffusion coefficient (D_{pa}) of the soluble profilin-actin complexes. At high concentrations of soluble actin, however, the rate is limited by two linked processes, each with its own (effective) diffusion coefficient. The elongation rate is still influenced by the re-charging of depleted polymerases, but it also depends on the rate at which fluctuating filament tips encounter actin-charged polymerases.

Finally, our formalism recaptures key features of previously published experimental data. Specifically, Bieling (2018) found that the rate of surface-mediated polymerization increases linearly from 0 to 2.75-times the rate of solution-mediated elongation as WAVE1 surface density increases from 0 to 1850/ μm^2. These experiments were performed in the presence of 1 μM soluble profilin-actin. Given this low actin concentration and relatively low WAVE1 surface density, the ratio of surface- to solution-mediated elongation rates will be described by the limiting case of **Eqn. 4a**. Assuming that the filament tip and polymerase molecule have similar interaction radii (i.e. $r_{tip} \sim r_{pa}$), then $R_{surf}/R_{soln} = 2.75 = n_{pol}/\pi$. From this, we estimate that each filament tip interacts with an average of 8.6 actin binding sites. If each WAVE1 molecule binds two profilin-actin complexes, then on average each filament is fed by 4.3 WAVE1 molecules. From this, we estimate that the surface interaction area of these filaments is ~2300 nm^2. This is approximately 36% of the interaction area of our model 300 nm filament oriented normal to a membrane surface (Appendix B). The smaller interaction area likely reflects the significant difference in geometry. Specifically, the filaments in the Bieling experiments elongated parallel to WAVE1-coated surfaces, so the interaction area traced by their fluctuating tips was most likely a “croissant” shape, rather than a radially symmetrical disc. In addition, these filaments were typically several microns long and the distance between their growing barbed ends and the nearest point of surface tethering was likely longer than 300 nm, leading to larger RMS tip deviations.

<u>Appendix A.</u>
List of variables and parameters

λ_{p-} Persistence Length of an actin filament
L Length of actin filament
D_{pa} Diffusion coefficient of soluble profilin-actin complexes
D_{tip} Effective diffusion coefficient of thermally fluctuating actin filament tip
r_{disc} Root Mean Square (RMS) deflection of membrane-adjacent filament tip
r_{tip} Capture radius of the barbed end of an actin filament
r_{pol} Effective profilin-actin capture radius of a surface-bound polymerase
n_{pol} Number of polymerase molecules inside a membrane-interaction region
c_o Actin monomer concentration
$k_{on}c_o$ Rate of loading profilin-actin onto a surface-associated polymerase site
d_o Total surface density of profilin-actin binding sites (/μm^2)
d_{pa} Surface density of occupied profilin-actin binding sites (/μm^2)
R_{soln} Rate of soluble profilin-actin monomers encountering a filament tip
R_{2D} Rate of surface-associated profilin-actin encountering a nearby filament tip
R_{disc} Rate of soluble monomers encountering the membrane-interaction disc
R_{surf} Rate of surface-associated profilin-actin encountering a nearby filament tip
E_{soln} Filament elongation rate from soluble profilin-actin monomers
E_{surf} Filament elongation rate from surface-associated profilin-actin
E_{total} Filament elongation rate from soluble *and* surface-associated profilin-actin
f_{surf} Fraction of filamentous actin incorporated from surface polymerases
f_{OL} Fractional overlap of membrane-interaction regions of adjacent filaments
n_{eff} Effective number of competing filaments in a membrane interaction region
x_{ff} Distance between the equilibrium positions of two filaments tips

Appendix B.
Size of the *membrane interaction disc* traced by fluctuating filament tips

Filaments in a functional branched actin network generally range between 150-800 nm in length (Svitkina, 1999; Akin, 2008; Koestler, 2009), much shorter than their mechanical persistence length (λ_p). At these lengths, a filament behaves as a relatively stiff beam (Fig. B1). If we consider only small-amplitude, planar bends, deflection of the filament tip follows Hooke's Law, meaning that displacement from equilibrium (r) is directly proportional to applied force (F) :

$$F = \kappa r$$

Where the effective spring constant (κ) depends on the persistence length (λ_p) and actual filament length (L):

$$\kappa = k_B T \left(\frac{3\lambda_p}{L^3} \right)$$

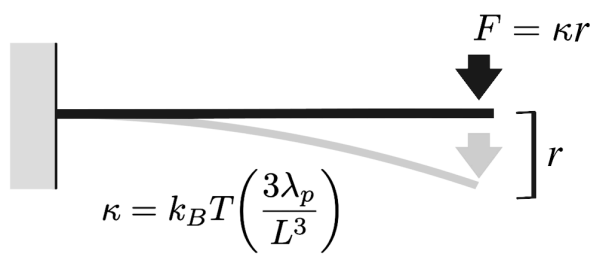

Figure B1. Small deflection bending of a stiff beam. The deflection is proportional to applied force, with an effective spring constant that depends on beam length and persistence length.

Where T is absolute temperature and k_B Boltzman's constant. From this, we can calculate the energy stored in the bent polymer:

$$E = \frac{1}{2}\kappa r^2 = k_B T \left(\frac{3\lambda_p}{2L^3} \right) r^2$$

If the average energy stored the bent polymer is $k_B T$, this yields:

$$k_B T = k_B T \left(\frac{3\lambda_p}{2L^3} \right) \langle r^2 \rangle$$

And the root-mean square (RMS) deviation of the tip is:

$$\sqrt{\langle r^2 \rangle} = \sqrt{\frac{2L^3}{3\lambda_p}}$$

Assuming an average filament length (L_{av}) of ~110 promoters (~300 nm), measured from the free barbed end to the network-anchored pointed end, the root-mean square (RMS) displacement of the tip will be ~45 nm.

Appendix C.
Numerical solution of Fick's equation in two dimensions with polymerase refilling from solution.

In this section we calculate a two-dimensional 'Smoluchowski limit' on the rate at which a growing filament tip interacts with profilin-actin-charged polymerase molecules on a membrane surface. We treat the filament tip as a circular hole whose radius (r_{tip}) represents the effective radius of interaction with polymerase-bound actin. For boundary conditions, we assume that the density of actin-bound polymerases is zero at the edge of the filament ($d_{pa}(r_{tip}) = 0$), and equal to the total polymerase density (d_o) at long distances ($d_{pa}(\infty) = d_o$). We then use Fick's law to calculate the gradient of occupied polymerase molecules around the filament tip (Von Smoluchowski, 1917; Debye, 1942). Note that this approach is valid regardless of which species —filament or polymerase— undergoes diffusive motion (Debye, 1942).

If we neglect refilling of depleted polymerases by soluble profilin-actin complexes, and assume a radially symmetrical distribution of actin-bound polymerases around the filament tip, the steady-state form of Fick's Law in two dimensions is:

$$D_{tip}\frac{1}{r}\left[\frac{\partial}{\partial r}\left(r\frac{\partial d_{pa}}{\partial r}\right)\right] = 0$$

Where D_{tip} is the diffusion coefficient of the filament tip walking across the membrane surface. Unlike the three-dimensional case, this partial differential equation has no solution that satisfies the given boundary conditions. If, however, we assume that unoccupied polymerase sites are refilled from a constant reservoir of soluble profilin-actin, the steady-state distribution of occupied polymerases satisfies:

$$D_{tip}\frac{1}{r}\left[\frac{\partial}{\partial r}\left(r\frac{\partial d_{pa}}{\partial r}\right)\right] = k_{on}c_o\left(d_o - d_{pa}\right) \qquad \textbf{Eqn. C1}$$

The right side of this equation represents the rate at which unoccupied polymerases are recharged from solution. This depends on the concentration of

unoccupied polymerases (d_o-d_{pa}), the solution concentration of profilin-actin complexes (c_o), and a rate constant (k_{on}) for binding of soluble proteins to membrane-associated sites (Berg, 1977). We found no simple analytical solution to this equation, so we solved it by numerical simulation. Briefly, we modeled diffusion in radial coordinates on a set of concentric rings, each with a fixed width (δ). Given values for δ and filament tip diffusion coefficient (D_{tip}) we chose a time step (τ) such that $\tau = \delta^2/D_{tip}$. We set up an initial, uniform distribution of loaded polymerases, with $d_{pa} = d_o$ for all $r > r_{tip}$, and stable boundary conditions of $d_{pa} = 0$ at $r = r_{tip}$ and $d_{pa} = d_o$ at $r > 1000\delta$. At each time step, τ, we assumed that the molecules in each concentric ring move inward or outward with the ratio of in-to-out determined by the areas of the adjacent rings. We then calculated the number of profilin-actin complexes recruited to each ring from solution by multiplying the area of the ring by the density of unoccupied polymerases, the solution concentration of profilin-actin, the rate constant for polymerase charging and the time increment: $k_{on}c_o(d_o\text{-}d_{pa})\tau$. We obtained the steady-state distribution of actin-charged polymerases by iterating time steps until the change in distribution became negligible. We validated this approach by

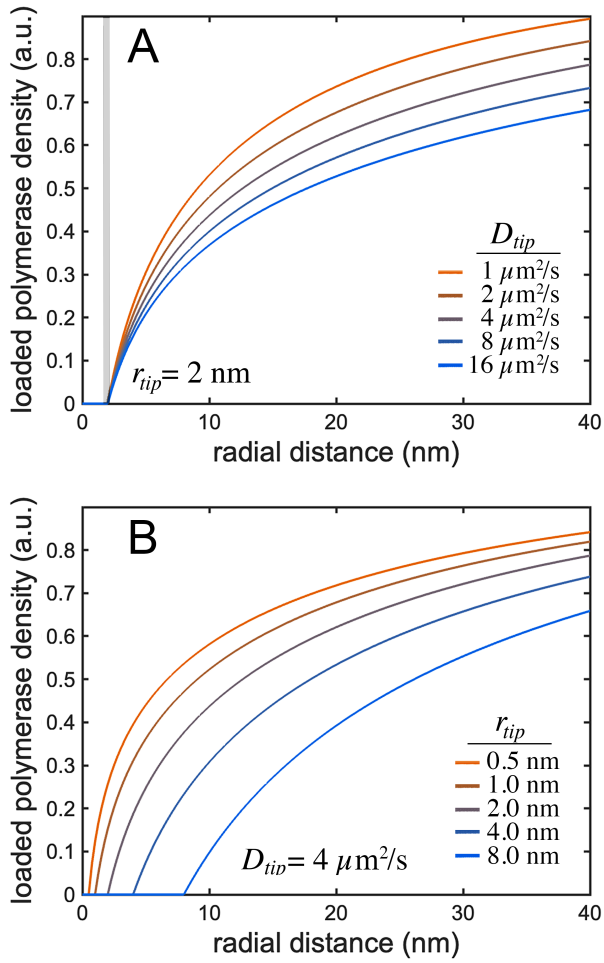

Figure C1. Steady-state distributions of actin-charged polymerases around an absorbing filament tip, determined by numerical simulation with various parameter values: (A) varying diffusion coefficients and (B) varying capture radii of the filament tip. For all conditions, c_o=100μM.

$$R_{2D} \approx \left[2.6 D_{tip}^{0.875} \cdot \left(r_{tip}^2 k_{on} c_o\right)^{0.125}\right] d_o = k'_+ d_o \qquad \textbf{Eqn. C2}$$

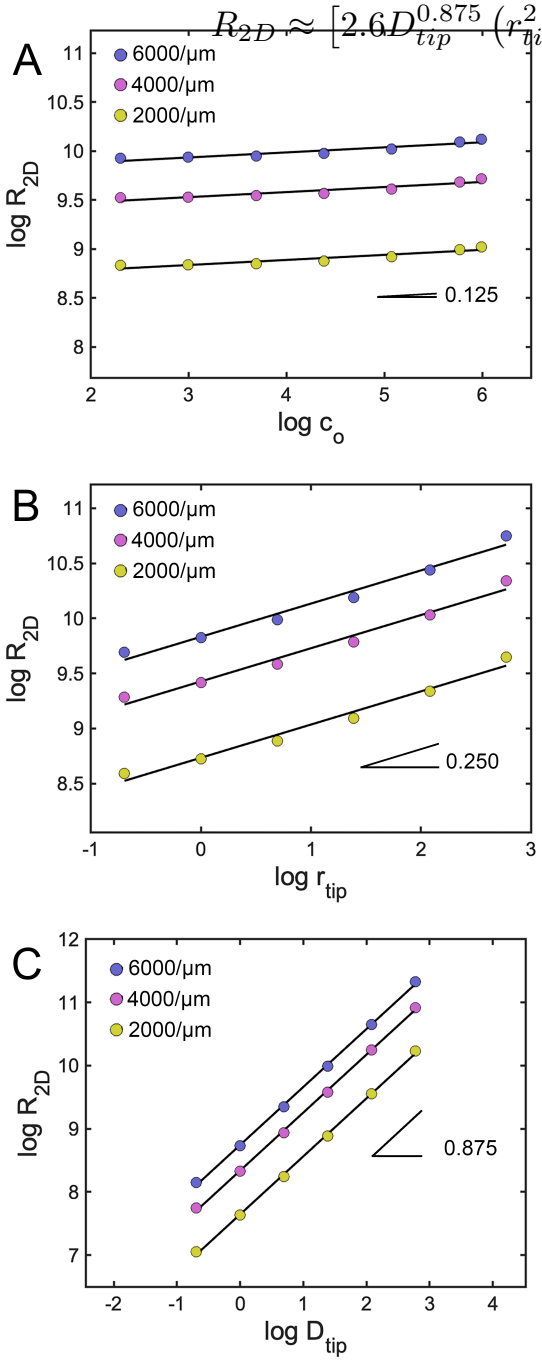

Figure C2. Log-log plots of 2D filament encounter rate (R_{2D}) versus key parameter values. (A) R_{2D} vs. soluble profilin-actin concentration (c_o). Slope: 0.125. (B) R_{2D} vs. filament capture radius (r_{tip}). Slope: 0.25. (C) R_{2D} vs. tip diffusion coefficient (D_{tip}). Slope: 0.875. Baseline parameter values: c_o=100 μM; r_{tip}=2 nm;

simulating diffusion into a three-dimensional, spherical absorber and comparing the results to von Smoluchowski (1917).

Our simulations produced stable distributions of actin-charged polymerases around the filament tip (Figure C1). From these distributions we calculated the flux of actin into the filament (R_{2D}) at different values of the relevant parameters ($k_{on}c_o$, r_{tip}, D_{tip}, and d_o).

Across physiologically relevant values of each parameter (Table C1), the interaction rate was well approximated as a simple power law (Figure C2, Table C1). Combining the dependences on all of the parameters into a single equation yields:

The above equation can be rearranged

$$R_{2D} \approx \left[2.6 D_{tip} \left(\frac{r_{tip}^2 k_{on} c_o}{D_{tip}}\right)^{0.125}\right] d_o = k' d_o$$

into a slightly more interpretable form:

The product of diffusion coefficient and surface actin density ($D_{tip}d_o$) is proportional to the rate of collision between a polymerase and the filament tip, while the unitless term in parentheses can be interpreted as the number of times a polymerase can be loaded with profilin-actin from solution during a single collision event. We have no physical interpretation of the exponent (~1/8). The term in square brackets has the form of a rate constant (k').

Table C1. Parameter ranges and exponents

Parameter	**Range**	**Exponent**
c_o	10-400 μM	0.125
r_{tip},	0.5-8 nm	0.25
D_{tip}	1-16 μm^2/s	0.875
d_o	2000-6000/μm^2	1.0

Acknowledgments. This work was supported by grants from the National Institutes of Health (1R35 GM118119) and the Howard Hughes Medical Institute. We are grateful to members of the Mullins Lab for helpful discussions and critical readings of the manuscript, especially Sam Lord and Arthur Charles-Orszag. We are also indebted to Alex Mogilner and Rob Phillips for critical readings of early drafts of this manuscript and useful discussions which significantly improved both argument and the presentation.

\displaystyle R_{2D} \approx \left[2.6 D_{tip}\left(\frac{r_{tip}^2k_{on}c_o}{D_{tip}} \right)^{0.125} \right]d_o=k'd_o

$$R_{2D} \approx \left[2.6 D_{tip}\left(\frac{r_{tip}^2k_{on}c_o}{D_{tip}} \right)^{0.125} \right]d_o=k'd_o$$

References

Abbott EA. (1884). “Flatland: a Romance of Many Dimensions.” London UK: Seeley & Co.

Adam, G. and Delbruck, M. (1968) Reduction of dimensionality in biological diffusion processes, in “Structural Chemistry and Molecular Biology” (Freeman, San Francisco), pp. 198–215.

Akin O, Mullins RD. (2008) Capping protein increases the rate of actin-based motility by promoting filament nucleation by the Arp2/3 complex. *Cell.* **133**(5):841-51.PMID: 18510928.

Berro J, Sirotkin V, Pollard TD. (2010) Mathematical modeling of endocytic actin patch kinetics in fission yeast: disassembly requires release of actin filament fragments. *Mol Biol Cell.* **21**(16):2905-15. PMID: 20587776.

Bénichou O, Chevalier C, Klafter, J, Meyer B, Voituriez R. (2010) Geometry-controlled kinetics. *Nat. Chem.* **2:**472–477.

Berg HC, Purcell EM. (1977) Physics of chemoreception. *Biophys. J.* **20**:193–219.

Berg OG, von Hippel PH. (1985) Diffusion-controlled macromolecular interactions. *Annu. Rev. Biophys. Biophys. Chem.* **14**:131–160.

Bieling P, Li TD, Weichsel J, McGorty R, Jreij P, Huang B, Fletcher DA, Mullins RD. (2016) Force Feedback Controls Motor Activity and Mechanical Properties of Self-Assembling Branched Actin Networks. *Cell.* **164**(1-2):115-127. PMID: 26771487.

Bieling P, Hansen SD, Akin O, Li TD, Hayden CC, Fletcher DA, Mullins RD. (2018) WH2 and proline-rich domains of WASP-family proteins collaborate to accelerate actin filament elongation. *EMBO J.* **37**(1):102-121. PMID: 29141912.

Bisi S, Disanza A, Malinverno C, Frittoli E, Palamidessi A, Scita G. (2013) Membrane and actin dynamics interplay at lamellipodia leading edge. *Curr Opin Cell Biol.* **25**(5):565-73. PMID: 23639310.

Breitsprecher D, Kiesewetter AK, Linkner J, Urbanke C, Resch GP, Small JV, Faix J. (2008) Clustering of VASP actively drives processive, WH2 domain-mediated actin filament elongation. *EMBO J.* **27**(22):2943-54. PMID: 18923426.

Clark AG, Miller AL, Vaughan E, Yu HY, Penkert R, Bement WM. (2009) Integration of single and multicellular wound responses. *Curr Biol.* **19**(16):1389-95. PMID: 19631537.

Courtemanche N, Pollard TD. (2013) Interaction of profilin with the barbed end of actin filaments. *Biochemistry* **52:**6456–6466.

Debye, P. (1942) Reaction rates in ionic solutions. *Trans. Electrochem. Soc.* **82**:265.

Drenckhahn D, Pollard TD. (1986) Elongation of actin filaments is a diffusion-limited reaction at the barbed end and is accelerated by inert macromolecules. *J Biol Chem.* **261**(27):12754-8. PMID: 3745211.

Efimova N, Svitkina TM. (2018) Branched actin networks push against each other at adherens junctions to maintain cell-cell adhesion. *J Cell Biol.* **217**(5):1827-1845. PMID: 29507127.

Fox JE. (1993) The platelet cytoskeleton. *Thromb Haemost.* **70**(6):884-93. PMID: 8165606.

Fritz-Laylin LK, Lord SJ, Mullins RD. (2017) WASP and SCAR are evolutionarily conserved in actin-filled pseudopod-based motility. *J Cell Biol.* **216**(6):1673-1688. PMID: 28473602.

Fujiwara, I., Vavylonis, D., and Pollard, T. D. (2007). Polymerization kinetics of ADP- and ADP-Pi-actin determined by fluorescence microscopy. *Proc.Natl. Acad. Sci. USA.* **104:**8827– 8832. PMID: 17517656.

Funk J, Merino F, Venkova L, Heydenreich L, Kierfeld J, Vargas P, Raunser S, Piel M, Bieling P. (2019) Profilin and formin constitute a pacemaker system for robust actin filament growth. *Elife.* **8**:e50963. PMID: 31647411.

Garner RM, Theriot JA. (2022) Leading edge maintenance in migrating cells is an emergent property of branched actin network growth. *Elife.* **11**:e74389. PMID: 35275060.

Hill T, Kirschner M. (1982) Bioenergetics and kinetics of microtubule and actin filament assembly and disassembly. *Int. Rev. Cytol.* **78**:1-125. PMID: 6128332.

Hansen SD, Mullins RD. (2010) VASP is a processive actin polymerase that requires monomeric actin for barbed end association. *J Cell Biol.* **191**(3):571-84. PMID: 21041447.

Huang WYC, Boxer SG, Ferrell JE Jr. (2024) Membrane localization accelerates association under conditions relevant to cellular signaling. *Proc Natl Acad Sci USA.* **121**(10):e2319491121. PMID: 38427601.

Hug C, Jay PY, Reddy I, McNally JG, Bridgman PC, Elson EL, and Cooper JA. (1995) Capping protein levels influence actin assembly and cell motility in *dictyostelium. Cell* **81:**591–600.

Kabsch W, Mannherz HG, Suck D, Pai EF, Holmes KC. (1990) Atomic structure of the actin:DNase I complex. *Nature*. **347**(6288):37-44. PMID: 2395459.

Kaiser DA, Vinson VK, Murphy DB, Pollard TD. (1999) Profilin is predominantly associated with monomeric actin in Acanthamoeba. *J Cell Sci*. **112**(21):3779-90. PMID: 10523513.

Kast DJ, Zajac AL, Holzbaur EL, Ostap EM, Dominguez R. (2015) WHAMM Directs the Arp2/3 Complex to the ER for Autophagosome Biogenesis through an Actin Comet Tail Mechanism. *Curr Biol*. **25**(13):1791-7. PMID: 26096974.

Kiuchi T, Nagai T, Ohashi K, Mizuno K, (2011) Measurements of spatiotemporal changes in G-actin concentration reveal its effect on stimulus-induced actin assembly and lamellipodium extension. *J. Cell Biol*. **193:**365–380.

Koestler SA, Rottner K, Lai F, Block J, Vinzenz M, Small JV. (2009) F- and G-actin concentrations in lamellipodia of moving cells. *PLoS One*. **4**(3):e4810. PMID: 19277198.

Koronakis V, Hume PJ, Humphreys D, Liu T, Hørning O, Jensen ON, McGhie EJ. (2011) WAVE regulatory complex activation by cooperating GTPases Arf and Rac1. *Proc Natl Acad Sci USA*. **108**(35):14449-54. PMID: 21844371.

Kovar DR, Harris ES, Mahaffy R, Higgs HN, Pollard TD. (2006) Control of the assembly of ATP- and ADP-actin by formins and profilin. *Cell*. **124**(2):423-35. PMID: 16439214.

Kudryashova E, Ankita, Ulrichs H, Shekhar S, Kudryashov DS. (2022) Pointed-end processive elongation of actin filaments by Vibrio effectors VopF and VopL. *Sci Adv*. **8**(46):eadc9239. PMID: 36399577.

Li TD, Bieling P, Weichsel J, Mullins RD, Fletcher DA. (2022) The molecular mechanism of load adaptation by branched actin networks. *Elife*. **11**:e73145. PMID: 35748355.

Machesky LM, Mullins RD, Higgs HN, Kaiser DA, Blanchoin L, May RC, Hall ME, Pollard TD. (1999) Scar, a WASp-related protein, activates nucleation of actin filaments by the Arp2/3 complex. *Proc Natl Acad Sci USA*. **96**(7):3739-44. PMID: 10097107.

McCloskey MA, Poo MM. (1986) Rates of membrane-associated reactions: reduction of dimensionality revisited. *J. Cell Biol*. **102:**88–96.

Mejillano, M.R., Kojima, S., Applewhite, D.A., Gertler, F.B., Svitkina, T.M., and Borisy GG. (2004) Lamellipodial versus filopodial mode of the actin nano-machinery: pivotal role of the filament barbed end. *Cell* **118:**363–373.

Millius A, Watanabe N, Weiner OD. (2012) Diffusion, capture and recycling of SCAR/WAVE and Arp2/3 complexes observed in cells by single-molecule imaging. *J Cell Sci.* **125**(Pt 5):1165-76. PMID: 22349699.

Mogilner A, Oster G. (1996) Cell motility driven by actin polymerization. *Biophys J.* **71**(6):3030-45. PMID: 8968574.

Mogilner A, Edelstein-Keshet L. (2002) Regulation of actin dynamics in rapidly moving cells: a quantitative analysis. *Biophys. J.* **83:**1237–1258.

Mooren OL, Galletta BJ, Cooper JA. (2012) Roles for actin assembly in endocytosis. *Annu Rev Biochem.* **81**:661-86. PMID: 22663081.

Mullins RD, Bieling P, Fletcher DA. (2018) From solution to surface to filament: actin flux into branched networks. *Biophys. Rev.* **10:**1537–1551.

Northrup SH, Erickson HP. (1992) Kinetics of protein-protein association explained by Brownian dynamics computer simulation. *Proc Natl Acad Sci USA.* **89**(8):3338-42. PMID: 1565624.

Novak IL, Slepchenko BM, Mogilner A., (2008) Quantitative analysis of G-actin transport in motile cells. *Biophys. J.* **95:**1627–1638.

Oda T, Iwasa M, Aihara T, Maéda Y, Narita A. (2009) The nature of the globular- to-fibrous-actin transition. *Nature.* **457**(7228):441-5. PMID:19158791.

Pollard TD, Cooper JA. (1984) Quantitative analysis of the effect of Acanthamoeba profilin on actin filament nucleation and elongation. *Biochemistry.* **23**(26):6631-41. PMID: 6543322.

Pollard TD. (1986) Rate constants for the reactions of ATP- and ADP-actin with the ends of actin filaments. *J Cell Biol.* **103**(6 Pt 2):2747-54. PMID: 3793756.

Pollard TD, Blanchoin L, Mullins RD. (2000) Molecular mechanisms controlling actin filament dynamics in nonmuscle cells. *Annu. Rev. Biophys. Biomol. Struct.* **29**: 545–576.

Pruyne D, Evangelista M, Yang C, Bi E, Zigmond S, Bretscher A, Boone C. (2002) Role of formins in actin assembly: nucleation and barbed-end association. *Science.* **297**(5581):612-5. PMID: 12052901.

Romero S, Le Clainche C, Didry D, Egile C, Pantaloni D, Carlier MF. (2004) Formin is a processive motor that requires profilin to accelerate actin assembly and associated ATP hydrolysis. *Cell.* **119**(3):419-29. PMID: 15507212.

Schaus TE, Taylor EW, Borisy GG. (2007) Self-organization of actin filament orientation in the dendritic-nucleation/array-treadmilling model. *Proc Natl Acad Sci USA*. **104**(17):7086-91. PMID: 17440042.

Schutt CE, Myslik JC, Rozycki MD, Goonesekere NC, Lindberg U. (1993) The structure of crystalline profilin-beta-actin. *Nature.* **365**(6449):810-6. PMID: 8413665.

Svitkina TM, Borisy GG. (1999) Arp2/3 complex and actin depolymerizing factor/cofilin in dendritic organization and treadmilling of actin filament array in lamellipodia. *J Cell Biol.* **145**(5):1009-26. PMID: 10352018.

Tilney LG, Bonder EM, Coluccio LM, Mooseker MS. (1983) Actin from Thyone sperm assembles on only one end of an actin filament: a behavior regulated by profilin. *J Cell Biol.* **97**(1):112-24. PMID: 6863386.

Von Smoluchowski, M., (1917) Attempt to derive a mathematical theory of coagulation kinetics in colloidal solutions. *Z. Phys. Chem.* **92**:129

Welch MD, Mullins RD. (2002) Cellular control of actin nucleation. *Annu Rev Cell Dev Biol.***18**:247-88. PMID: 12142287.

Windisch B, Bray D, Duke T. (2006) Balls and chains—a mesoscopic approach to tethered protein domains. *Biophys J.* **91**(7):2383-92. PMID: 16829557.

Wu M, Marchando P, Meyer K, Tang Z, Woolfson DN, Weiner OD. (2024) The WAVE complex forms linear arrays at negative membrane curvature to instruct lamellipodia formation. *bioRxiv* 2024.07.08.600855.